Molecular Catalysis 531 (2022) 112683

Contents lists available at ScienceDirect

Molecular Catalysis

journal homepage: www.journals.elsevier.com/molecular-catalysis

Florol synthesis via Prins cyclization over hierarchical beta zeolites

Nataliya Shcherban [a,*], Roman Barakov [a], Basile Lasne [b], Päivi Mäki-Arvela [b], Mariya Shamzhy [c], Igor Bezverkhyy [d], Johan Wärnå [b], Dmitry Yu. Murzin [b,*]

[a] L.V. Pisarzhevsky Institute of Physical Chemistry, National Academy of Sciences of Ukraine, 31 pr. Nauky, Kyiv 03028, Ukraine
[b] Johan Gadolin Process Chemistry Centre, Faculty of Science and Engineering, Åbo Akademi University, Henriksgatan 2, Turku/Åbo 20500, Finland
[c] Department of Physical and Macromolecular Chemistry, Faculty of Science, Charles University, Hlavova 2030, Prague 2 12840, Czech Republic
[d] Laboratoire Interdisciplinaire Carnot de Bourgogne, UMR 6303 CNRS-Université de Bourgogne-Franche Comté, 9 Av. A. Savary, BP 47870, Dijon Cedex 21078, France

ARTICLE INFO

Keywords:
Hierarchical zeolite
Prins cyclisation
Tetrahydropyranol
Florol, Acid sites

ABSTRACT

A set of hierarchical beta zeolites with variable Si/Al ratios, nanoparticle sizes, textural and acidic properties was prepared using a hydrothermal treatment of a concentrated alkali metal-free protic acid-containing zeolite gel-precursor. The obtained catalysts were investigated in the Prins cyclization of isovaleraldehyde with isoprenol yielding a commercially valuable tetrahydropyranol (Florol). The highest yield of the desired product (55.4%) was achieved over a zeolite catalyst possessing moderate acidity, developed mesoporosity (V_{meso} 0.60 cm^3/g) and a high external surface area (290 m^2/g). Preferable formation of substituted tetrahydropyranol over weak- and medium-strength Brønsted acid sites, on the one hand, and generation of the undesired dehydration products mainly over strong Brønsted acid sites, on the other hand, occurring in parallel routes were supported by the kinetic analysis of the reaction network.

1. Introduction

Hierarchical zeolites are one of the most perspective acidic catalytic materials consisting of a crystalline network that possess not only uniform micropores, but also a secondary meso- or macro-porosity, enabling conversion of bulky organic molecules [1–4]. Various methods are used to obtain hierarchical zeolites [5], such as synthesis in the presence of hard templates (carbon nanoparticles and nanofibers, polystyrene spheres) [6], non-ionic and cationic polymers [7,8], amphiphilic organosilanes and silylating agents [9,10], multi-quaternary ammonium surfactants [11]. However, these methods have several drawbacks such as a high cost of templates and structure-directing agents forming mesopores (mesoporogens), a relatively broad mesopore size distribution, low crystallinity, and a limited concentration of acid sites in the obtained materials. Hierarchical micro-mesoporous zeolites consisting of beta nanoparticles (15 – 40 nm) were obtained *via* hydrothermal treatment of concentrated zeolite reaction mixtures (H_2O/Si = 2.5 – 14) without utilization of complex structure-directing agents [12–14]. Formation of a large number of zeolite nuclei during hydrothermal treatment of the TEAOH-containing concentrated reaction mixtures favors the packing of the nanoparticles over their crystal growth, thus resulting in highly porous hierarchical materials with intercrystalline mesoporosity instead of microporous catalysts. The micelles of cetyltrimethylammonium bromide were shown to additionally limit the growth of zeolite nanoparticles during the hydrothermal treatment [15,16]. Resulting materials with a high concentration of acid sites on the external surface demonstrated enhanced catalytic activity in the Prins–Friedel–Crafts reaction of butyraldehyde with 3-buten-1-ol and anisole [12], Prins cyclisation of (-)-isopulegol with acetone [17], α-pinene oxide isomerization [18], as well as tetrahydropyranylation of bulk alcohols [15]. In this study, a simple, straightforward and cost efficient method for the synthesis of hierarchical beta zeolites with a variable Si/Al ratio, nanoparticle sizes, textural properties (micropore and mesopore volumes, mesopore diameter, total specific surface area, external surface area) and acid site concentrations is proposed. In contrast to the previous reports, conditions of the hydrothermal treatment were optimized for the preparation of hierarchical zeolites in alkali metal-free protic acid-containing mixtures which allows to obtain H-forms of hierarchical beta zeolites directly after calcination without additional ion-exchange. Addition of a protic acid to the reaction mixture contributes to slowing down crystallization and limiting growth of the zeolite nanoparticles.

The catalytic performance of the prepared hierarchical zeolite catalysts was studied in the Prins cyclization reaction between biomass-

* Corresponding authors.
E-mail addresses: nataliyalisenko@ukr.net (N. Shcherban), dmurzin@abo.fi (D.Yu. Murzin).

https://doi.org/10.1016/j.mcat.2022.112683
Received 1 July 2022; Received in revised form 5 September 2022; Accepted 10 September 2022
Available online 19 September 2022

derived isoprenol and isovaleraldehyde resulting in a commercial perfume ingredient (Florol®) [19,20]. Besides the desired tetrahydropyranol (THP), this reaction can also give several dehydration products (DHP) (Scheme 1) capable of subsequent reactions with the initial substrates (IVA or IP) resulting in trimers.

According to the knowledge of the authors, catalytic behavior of hierarchical beta zeolites in the Prins cyclisation of isoprenol and isovaleraldehyde was not previously reported in the open literature. Preparation of Florol (also called Florosa) was reported using several homogeneous and heterogeneous catalysts. In particular, an ion-exchange resin Amberlyst-15 was found to be efficient for the Prins cyclization to yield 4-hydroxytetrahydropyrans, including Florol (51% yield, 70 – 80 °C, solvent-free conditions) [21]. Similarly, sulfonated hyper-cross-linked polyacetylene-type micro/mesoporous polymers were discovered to catalyze the Prins cyclization of isoprenol and benzaldehyde even more effectively compared to Amberlyst-15 due to the enhanced transport of the reactants to the active sites [22]. Application of heteropoly acids *per se* and immobilized on silica MCM-41 afforded 96% selectivity (at 70% conversion of isovaleraldehyde) towards the desired tetrahydropyranol at 80 °C in water as a solvent [23]. 80% yield of Florol was reported over a silica-supported heteropoly acid under mild conditions using green solvents (dimethylcarbonate or diethylcarbonate) [24]. Deposition of MoO_3 onto silicas [25] or alumosilicates [26] providing a higher dispersion of the active phase resulted in ca. 50% selectivity towards the desired substituted tetrahydropyranol at 70 °C. Silica materials modified using iron nitrate were found to be active only in the formation of hemiacetal or acetal as side products. At the same time Fe-modified catalysts prepared by impregnation of silica gel with iron chloride demonstrated significantly better catalytic performance. Selectivity up to 70% to the desired product at 90 °C was attributed to a higher acidity [27]. At the same time modification of zeolites, namely Beta, with iron is accompanied with an increase in conversion of the initial reagents (benzaldehyde or butanal in the reaction with isoprenol) while selectivity toward the reaction products (tetrahydropyranols, dihydropyrans and acetals) was almost unchanged [28]. Prins cyclisation of isoprenol with several aldehydes was also studied over montmorillonite K10 showing for isovaleraldehyde, in particular, 61% selectivity towards the desired substituted tetrahydropyranol at 95% conversion at 70 °C in toluene [29]. Acid-modified clays such as halloysite, montmorillonite and illite were also found to be promising for cyclization of isoprenol with isovaleraldehyde providing 65 – 72% yield of tetrahydropyranol under solvent-free conditions [30]. Investigation of several conventional microporous Beta and USY zeolites with various Si/Al ratio in the above mentioned Prins reaction revealed that Beta zeolite with the SiO_2/Al_2O_3 ratio of 300 demonstrated the best catalytic performance reaching 72% selectivity at 99% conversion and 40 °C in dimethylcarbonate as a solvent [31].

Specifically, this work was devoted to the investigation of the influence of textural and acidic properties of synthesized hierarchical beta zeolites on their catalytic activity in the Prins cyclization of isovaleraldehyde with isoprenol, comparing the results with the previous studies of this reaction over heterogeneous catalysts and own studies focusing mainly on microporous beta zeolite [31]. Due to the presence of mesopores in hierarchical zeolites providing benefits in catalysis such as reduction of the steric limitations for converting bulky molecules exceeding the zeolite micropore size or increase in the rate of intracrystalline diffusion, these materials can be promising catalysts in the Prins cyclization of isovaleraldehyde with isoprenol.

2. Experimental part

2.1. Synthesis of the samples

Hierarchical beta zeolites (HBZ) were synthesized *via* hydrothermal treatment (HTT) of reaction mixtures with a composition of $1SiO_2$: xAl_2O_3:0.6TEAOH:0.2HCl:yH_2O ($x = 0.014$ or 0.025, $y = 3$, 10, 15, 20, Table 1) not containing extra templates or alkali metal cations. The tetraethylammonium hydroxide (TEAOH) solution (40 wt.%, Sigma-Aldrich, 6.42 g) and 0.57 g of hydrochloric acid (37 wt.%, Sigma-Aldrich) were added to distilled water. Then 1.74 g of fumed silica (0.2–0.3 μm average particle size, aggregate, Sigma-Aldrich) was added under vigorous stirring. After stirring for 30 min, 0.064 g (Si/Al = 35) of aluminum hydroxide (63.5 wt.% Al_2O_3, Acros Organics) or 0.113 g (Si/Al = 20) was added and the reaction mixture was stirred for 60 min. Then obtained reaction mixture was dried at 60 °C to reach the desired H_2O/SiO_2 molar ratio at 3 – 20 (HBZ-1 – HBZ-6, Table 1). Thereafter the reaction mixture was placed in a Teflon-lined stainless-steel autoclave and subjected to hydrothermal treatment at 140 °C for 7 days under static conditions. The solid product was then isolated by centrifugation, washed with 80 ml of distilled water (with portions of 20 ml) until the pH of the filtrate was below 8, dried in an oven at 60 °C, and calcined in a furnace at 550 °C for 5 h with a ramping rate 2 °C/min.

For investigation of the water effect on the catalytic performance, several spent catalysts were dried at 100 °C in an oven (considered as water-containing due to the presence of water in micropores) and treated at 250 °C in argon (considered as dry samples).

Table 1
Synthesis conditions, zeolite particle size and relative crystallinity of the samples.

Sample	Reaction mixture		Zeolite particle size[a] (nm)	Relative crystallinity (%)
	Si/Al	H_2O/Si		
HBZ-1	35	10	48±6	41
HBZ-2	35	20	14±1	24
HBZ-3	20	3	19±4	91
HBZ-4	20	10	182±21	86
HBZ-5	20	15	164±5	100
HBZ-6	20	20	265±26	95

[a] Zeolite particle size estimated from TEM images. σ value from the Gaussian distribution (Fig. A.9) represents the confidence interval.

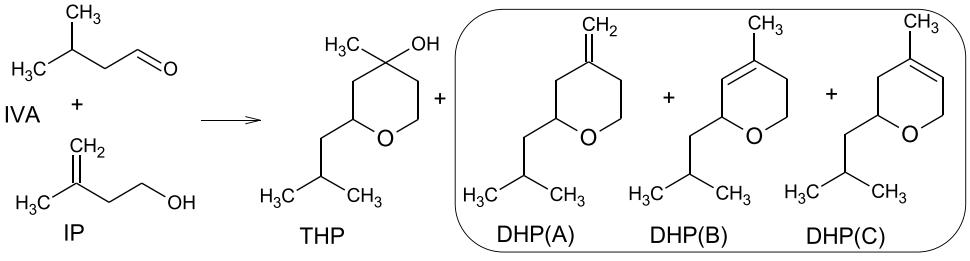

Scheme 1. Prins cyclization of isovaleraldehyde (IVA) and isoprenol (IP) resulting in tetrahydropyranol (2-isobutyl-4-methyl-tetrahydro-2H-pyran-4-ol, THP) and side dehydration products (DHP).

2.2. Characterization of samples

The phase composition of the samples was analyzed by powder X-ray diffraction (PXRD) on diffractometer D8 ADVANCE (Bruker AXS) with a graphite monochromator using CuK_α-radiation in the Bragg–Brentano geometry. According to the procedure given in Ref. [32], the relative crystallinity of the calcined samples was evaluated based on the area under the diffraction line in the $2\theta = 20 - 24^\circ$ range. For a qualitative evaluation, the crystallinity of HBZ-5 sample was set as equal to 100%, as this sample exhibited the largest area in the studied 2θ range.

The content of Si and Al in the materials was determined by ICP-OES (Thermo Scientific iCAP 7000) analysis. First, the mixture of 1.8 ml of HF, 5.4 ml of HCl, 1.8 ml of HNO_3 and 50 mg of the solid was transferred into a closed vessel, placed in the microwave oven, and heated. After cooling down, the surplus of HF was disposed by adding 13.5 ml of H_3BO_3 and by treatment under microwaves. Thereafter, the solutions were diluted with deionized water to 50 ml before analysis.

SEM images of the samples were obtained using field emission SEM JSM-7600F (JEOL). The images were recorded using the accelerating voltage of 1 – 30 kV and a secondary electron detector. A sample was loaded on the conductive graphitized support and the recording was carried out without preliminary deposition of conductive materials on the sample surface.

TEM images were obtained using field emission TEM JEM-2100F (JEOL) with an accelerating voltage of 200 kV. The samples were dispersed in ethanol in an ultrasonic bath for 5 min, and then the suspension was deposited onto a copper grid coated with an amorphous carbon film. The size of zeolite particles was determined without any digital processing of images. Zeolite particles in each agglomerate were distinguished using the limits between them which are visible in TEM images.

Solid-state ^{29}Si MAS NMR and ^{27}Al MAS NMR spectra were obtained using an Avance III HD (Bruker) spectrometer working with a 9.4 T standard-bore superconducting magnet at resonance frequency 79.5 MHz and 104.26 MHz, respectively. The samples were packed into a thin-wall 3.2 mm zirconia rotor, and rotated at a MAS rate of 15 kHz using a Bruker 3.2 mm HX CP-MAS probe. For recording ^{29}Si MAS NMR spectrum, a pulse of 1.9 μs (ca. 60° flip angle) with a relaxation delay of 20 s was applied and 2500 transients were averaged. The spectra were referenced to tetramethylsilane. For recording ^{27}Al MAS NMR spectrum, a pulse of 1.0 μs (B1 field approximately 95 kHz) with a relaxation delay of 1 s was applied and 2048 transients were averaged. The spectra were referenced to a saturated solution of $Al(NO_3)_3$ in D_2O. In all cases, no proton decoupling was applied.

Textural properties of the samples were evaluated from nitrogen adsorption-desorption isotherms measured using Micromeritics 3Flex static volumetric apparatus at –196 °C using 150–200 mg of the catalysts. Before the sorption measurements, all zeolites were degassed in a Smart Vac Prep instrument (Micromeritics) under vacuum at 250 °C (heating rate 1 °C/min) for 8 h. 42 data points with an equilibration interval 10 s were collected for each adsorption isotherm in the range $p/p_0 = 0 \div 1$. The specific surface area S_{BET} was evaluated using the updated Rouquerol criteria implemented in BETSI (Figs. A.1–6) [33]. The mesopore size distribution curves were obtained from the desorption branch of the isotherm using the Barrett-Joyner-Halenda (BJH) method [34]. The micropore volume (V_{micro}) and the external surface area (S_{ext}) were determined by the comparative *t-plot* method, as described in Refs. [35–37]. A reference isotherm, i.e. the dependence of the statistical thickness t on the relative pressure p/p_0 of a reference material, was evaluated from the data on macroporous silica (LiChrospher Si-1000) [37,38]. The adsorbed amount at a relative pressure p/p_0=0.98 was considered to reflect the total pore volume. Subsequently, the mesopore volume (V_{meso}) was determined as the difference between the total pore volume and the micropore volume.

The type, strength and concentration of the acid sites were determined by adsorption of pyridine monitored by FTIR spectroscopy [10, 39]. The spectra were collected using Nicolet iS50 (Thermo Fischer Scientific) spectrometer equipped with DTGS detector. Zeolite wafers were prepared following the methodology described in Ref. [40]. The samples were pressed into self-supported wafers with the cross-section of $S = 3$ cm^2, using a hydraulic bench press. For this purpose ca. 30 mg of the sample experienced a load of 1 tonne and a load time of 20 s. Prior to adsorption of the probe molecule, self-supported wafers of zeolite samples were activated *in situ* by evacuation at 450 °C for 4 h. Pyridine (Py) adsorption was done at 150 °C for 20 min at a partial pressure of 3 Torr, followed by 20 min evacuation at 150 – 450 °C with 100 °C steps. The concentration of Brønsted (BAS) and Lewis (LAS) acid sites was calculated from the integral intensities of the 1545 cm^{-1} band of the pyridinium ions (PyH^+) and the 1455 cm^{-1} band of pyridine coordinatively bonded to Lewis acid sites (PyL), respectively. The molar absorption coefficients recently determined on a high precision IR-microbalance system for BEA zeolite at 1.12 ± 0.16 cm/μmol (1545 cm^{-1}, PyH^+) and 1.71 ± 0.1 cm/μmol (1455 cm^{-1}, PyL) were used, respectively [40].

2.3. Catalytic tests

Prins cyclization of isoprenol with isovaleraldehyde was carried out in the liquid phase using a batch-mode operated glass reactor. Isoprenol (97%, Aldrich) and isovaleraldehyde (97%, Aldrich) were used as received without any further treatment. In a typical catalytic experiment, isoprenol (0.43 g, 5 mmol) and isovaleraldehyde (2.15 g, 25 mmol) were mixed with a solvent – dimethyl carbonate (99%, Aldrich) up to the total volume of 25 ml. The solvent was preheated at the reaction temperature (40 °C) under an inert gas (argon) atmosphere. The catalyst weight was 0.075 g and the stirring speed was 400 rpm to eliminate the impact of liquid-solid mass transfer limitations. The size of the powder was below 60 μm to avoid the limitations with the mass transfer the catalyst particles. The corresponding results from the calculation of the Weisz-Prater criterion are provided in the Discussion below. Prior to the reaction, the catalyst was heated in the reactor at 250 °C under an inert argon atmosphere for 30 min. The samples were taken at certain time intervals and analyzed by GC (Agilent Technologies 6890 N) equipped with an HP-5 column (30 m, 320 μm, 0.50 μm) applying the following temperature program: 60 °C (5 min) – 3 °C/min – 130 °C – 12 °C/min – 280 °C (10 min). The nature of the products was confirmed by GC–MS (Agilent Technologies 5973 N).

The conversion (X) of isoprenol (IP), selectivity (S_i) and the product yields (Y_i) were calculated based on the Eqs. (1)–(3).

$$X(\%) = \left[\left(C(IP)_0 - C(IP)_t\right) / C(IP)_0\right] * 100 \quad (1)$$

$$S_i(\%) = \left[C_i(product)_t \Big/ \sum C_i(product)_t\right] * 100 \quad (2)$$

$$Y_i(\%) = [X * S_i]/100 \quad (3)$$

where $C(IP)_0$ and $C(IP)_t$ are the concentrations (mol/l) of IP in the reaction mixture initially and after a certain time; $C_i(product)_t$ is the concentration (mol/l) of the specific product i at time t.

The concentrations of the reactant and product were determined using their response factors in GC analysis found from the multipoint calibration curves. The initial reaction rate was determined for the first 10 min of the reaction according to Eq. (4):

$$r_0(mmol / (\min * g_{cat})) = \left[n(IP)_0 - n(IP)_{10\min}\right]/m_{cat}/10(\min) \quad (4)$$

where $n(IP)_0$ and $n(IP)_{10\ min}$ are the amounts (mmol) of IP in the reaction mixture initially and after 10 min; m_{cat} is the mass of catalyst (0.075 g).

The turnover frequency ('TOF' or the number of converted IP moles per moles of accessible acid sites per unit time) was evaluated based on the total concentration of acid sites accessible for pyridine molecules

also for the first 10 min of the reaction:

$$TOF\left(min^{-1}\right) = \left[n(IP)_0 - n(IP)_{10\text{min}}\right] / n_{(acid\ \ sites\ \ in\ \ 75\ \ mg\ \ catalyst)} / 10(\text{min}) \quad (5)$$

where n(acid sites in 75 mg catalyst) is the amount (mmol) of BAS and LAS in 75 mg of the catalyst, as determined by FTIR of adsorbed pyridine.

The catalyst productivity after 3 h ('CP3h' or the total number of converted IP moles over accessible acid sites after 3 h) was calculated according to Eq. (6):

$$CP3h = \left[n(IP)_0 - n(IP)_{3h}\right] / n_{(acid\ \ sites\ \ in\ \ 75\ \ mg\ \ catalyst)} \quad (6)$$

where $n(IP)_{3h}$ is the amount (mmol) of *IP* in the reaction mixture after 3*h*.

3. Results and discussion

3.1. Catalyst characterization

Two sets of the hierarchical beta zeolites with various Si/Al molar ratios (20 and 35) in the reaction mixture were synthesized (HBZ-1, HBZ-2 and HBZ-3 – HBZ-6, Table 1). H_2O/Si ratio (3 – 20) was varied in these sets (Table 1) while maintaining other synthesis parameters. The chemical composition of the respective Al-poor and Al-rich catalysts was found in the ranges Si/Al = 43–46 (HBZ-1 and HBZ-2) and Si/Al=18–22 (HBZ-3-HBZ-6).

Structure and morphology. The diffraction peaks in PXRD patterns of all calcined samples HBZ-1 – HBZ-6 (Figs. 1a and 2a) are referred to pure *BEA zeolite phase [41]. The Al-rich samples HBZ-3 – HBZ-6 have higher relative crystallinity (86 – 100%) compared to Al-poor materials HBZ-1 and HBZ-2 (24 – 41%). This result can be explained considering formation of Si–O^-defects for compensation of the positive charges of TEA^+ (7.6/unit cell [41]) in the as-synthesized samples. This positive charge is higher in comparison to the negative charges introduced by Al atoms in the tetrahedral $[Al(OSi)_4]^-$ framework positions even for Al-rich HBZ-5 and HBZ-6 (6.1 Al/unit cell for the Si/Al ratio 18). Thus, the negative charges of Si–O^-groups in connectivity defects are formed to compensate the positive charges of the organic cations [32]. The number of Si–O^-groups increases and the relative crystallinity of the sample decreases with increasing the Si/Al ratio in the material, i.e., for HBZ-1 and HBZ-2 samples. According to SEM and TEM (Figs. 1, 2, A.7–9, Table 1), HBZ-1 – HBZ-6 consist of beta zeolite particles with a size of 14 – 265 nm agglomerated in larger particles.

HBZ-1 and HBZ-2 samples obtained in the Al-poor reaction mixtures with the Si/Al molar ratio of 35 contain relatively small nanoparticles (14 – 48 nm), while the size of beta particles in HBZ-4 – HBZ-6 synthesized in the mixture with a higher aluminum content (Si/Al = 20) and similar H_2O/Si ratio = 10 – 20 was remarkably higher (164 – 265 nm). Notably, the size of nanoparticles in Al-rich samples decreases from 164 – 265 nm to 19 nm with decreasing the H_2O/Si molar ratio from 20 to 3 (Table 1). The result reveals that a low amount of water in the reaction mixture promotes formation of the zeolite nuclei, and their agglomeration in the dense packing of the particles, while decelerates the growth of nanoparticles into large crystals.

The local environment of the Si and Al atoms in the representative sample HBZ-3 was investigated by using ^{29}Si MAS NMR and ^{27}Al MAS NMR spectroscopy, respectively. The peak at –100 ppm in the ^{29}Si MAS NMR spectrum of this sample (Fig. A.10) is referred to a silicon atom in the tetrahedral coordination environment bonded through an oxygen atom with one Al atom or OH-group and three Si atoms (Q_3). The peak at –109 ppm is attributed to a silicon atom connected with 4Si atoms (Q_4) [42]. Most of Q_3 and Q_4 silicon atoms are located in the zeolite framework, as the fraction of the amorphous phase in the HBZ-3 sample is rather low (ca. 9%). The peaks at 54 ppm and 0 ppm present in the ^{27}Al MAS NMR spectrum of HBZ-3 sample (Fig. A.11), correspond to aluminum atoms in the tetrahedral (in the zeolite framework) and octahedral (extra-framework Al species) coordination environment, respectively [42]. The fraction of the extra-framework Al species (e.g., Al_2O_3 particles) in this sample is small.

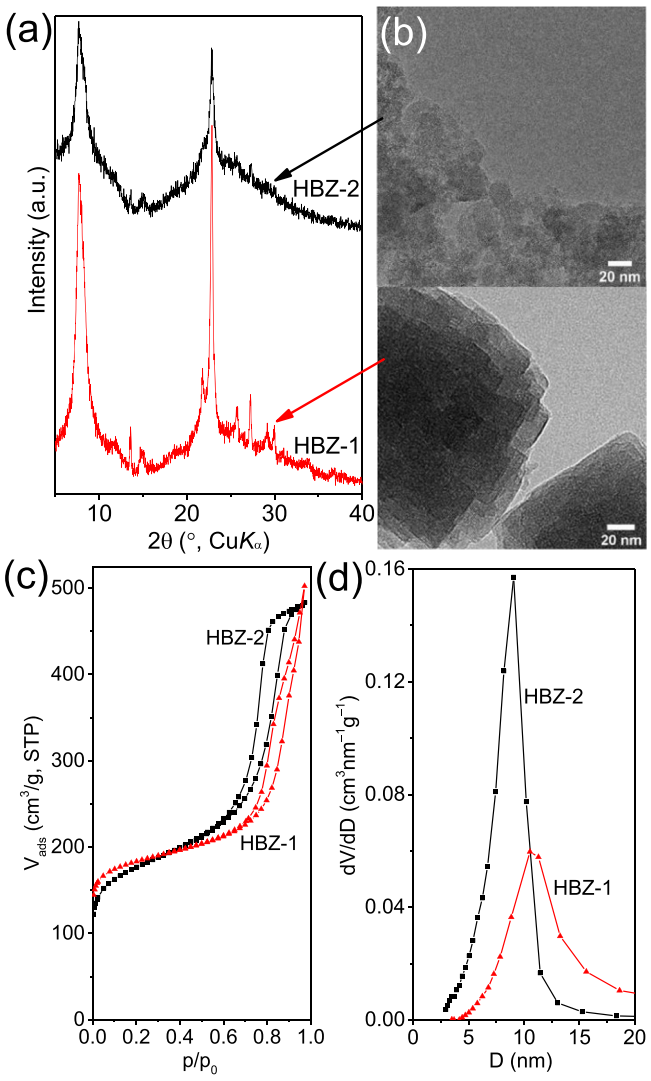

Fig. 1. PXRD patterns (a), TEM images (b), nitrogen adsorption-desorption isotherms at –196 °C (c) and mesopore size distribution (d) for the calcined samples HBZ-1 and HBZ-2.

Textural properties. Nitrogen adsorption-desorption isotherms for HBZ-1 – HBZ-6 materials (Figs. 1c and 2c) are of type *I*+IV according to IUPAC classification [43]. These isotherms show a high uptake of N_2 by micropores at low p/p_0 (<0.05). The presence of the hysteresis loop of the H_1 type (for HBZ-2) and H_3 type (for all other samples) at p/p_0 0.45 – 0.97 in these isotherms is associated with the nitrogen condensation in the interparticle voids with a size of 9 – 32 nm (Table 2) formed due to the agglomeration of beta zeolite nanoparticles. The H_3 type hysteresis loop also indicates the unrestricted adsorption at p/p_0 ca. 1.0. In addition, the tensile strength effect at p/p_0 ca. 0.45 is observed in the isotherms of HBZ-5 and HBZ-6. This points out on the presence of a very tortuous mesopore network in these samples [44]. The micropore volume was higher for high-crystalline materials (Tables 1 and 2) reaching 0.25 cm^3/g for the samples HBZ-4 – HBZ-6. Decrease in the zeolite particle sizes led to the increase in mesopore volume and the external surface area in a sequence HBZ-6 = HBZ-5 < HBZ-4 < HBZ-3. For example, highly crystalline HBZ-3 consisting of small nanoparticles (19 ±4 nm) is characterized by the well-developed mesoporosity (V_{meso} = 0.71 cm^3/g, S_{ext} = 240 m^2/g) and the largest total specific surface area

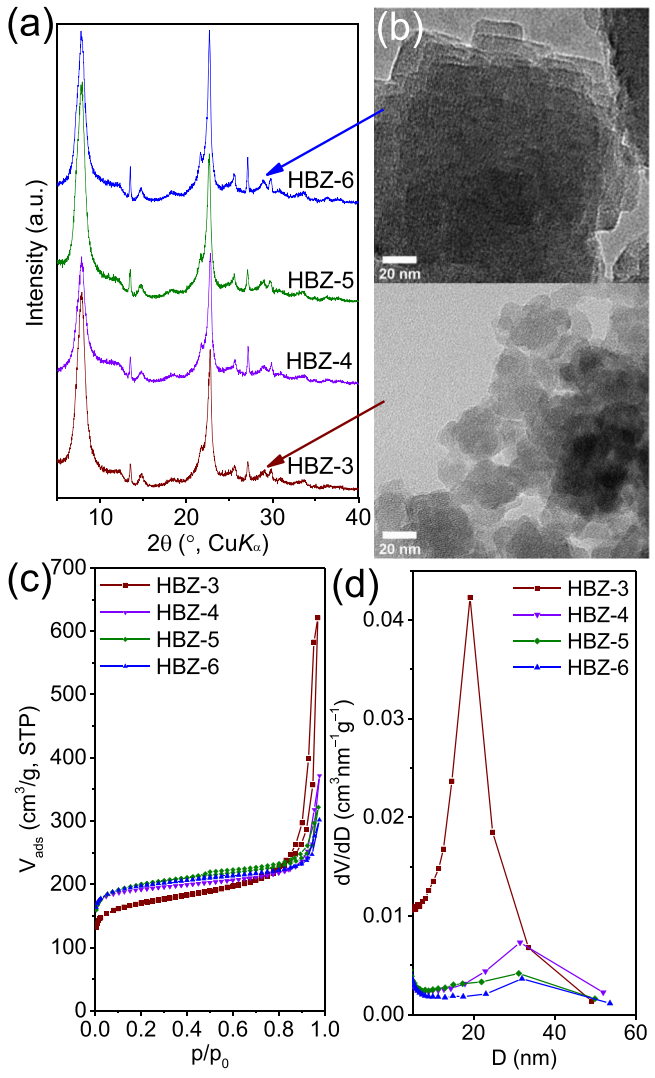

Fig. 2. PXRD patterns (a) of the calcined samples HBZ-3 – HBZ-6. TEM images (b) of the calcined samples HBZ-3 and HBZ-6. Nitrogen adsorption-desorption isotherms at –196 °C (c) and mesopore size distribution (d) for the samples HBZ-3 – HBZ-6.

Table 2
Characteristics of the porous structure (N_2, –196 °C) of the obtained samples.

Sample	V_{micro} [a] (cm^3/g)	V_{meso} [b] (cm^3/g)	D_{meso} [c] (nm)	S_{ext} [d] (m^2/g)	S_{BET} [e] (m^2/g)
HBZ-1	0.21[f]	0.57	11±3	160	698
HBZ-2	0.15	0.60	9 ± 1	290	649
HBZ-3	0.22	0.71	19±4	240	785
HBZ-4	0.25	0.33	31±9	100	752
HBZ-5	0.25	0.22	31±11	125	767
HBZ-6	0.25	0.22	32±8	125	766

[a] V_{micro}, micropore volume.
[b] V_{meso}, mesopore volume.
[c] D_{meso}, mesopore diameter. Gaussian distribution (standard deviation) was used to estimate the error in the mesopore diameter.
[d] S_{ext}, external surface area.
[e] S_{BET}, total specific surface area.
[f] Micropore diameter for the samples given in Table 2 is 0.65 nm.

(785 m^2/g) among the studied materials. The samples HBZ-1 and HBZ-2 prepared at low aluminum content (Si/Al = 35, H_2O/Si = 10 – 20) have a larger fraction of mesoporosity (Table 2) compared to HBZ-4 – HBZ-6 with a higher aluminum content in the reaction mixture (Si/Al = 20) and similar H_2O/Si, that has also been observed previously [32]. A more developed mesoporosity of the samples HBZ-1 and HBZ-2 is associated with formation of smaller zeolite nanoparticles (14 – 48) during the hydrothermal treatment as a result of better dissolution of aluminosilicate particles in the mixtures with an increased alkalinity (lower aluminum content).

Thus, according to the morphology analysis and textural properties of the obtained materials, they can be referred to agglomerated zeolite systems with a combination of zeolite microporosity and intercrystalline mesoporosity. The hierarchy of these materials is classified as type II with an interconnected pore system of two different pore sizes (micropores and mesopores), where the mesopores intersect the micropore system of zeolite nanoparticles [1,4].

Chemical composition and acidity. The aluminum content in HBZ-3 – HBZ-6 (Si/Al = 18 – 22, Table 3) is close to the composition of the reaction mixture (Si/Al = 20). In contrast, the Si/Al ratio in the low-crystalline HBZ-1 and HBZ-2 (Si/Al = 43 – 46) samples slightly exceeds the corresponding ratio in the reaction mixture (Si/Al = 35). The result is in line with previously reported difficulties in incorporation of aluminum into the amorphous phase [45].

Acidity of the samples was characterized by FTIR after pyridine adsorption (Tables 3 and A.1). The total concentration of acid sites in the samples increases with decreasing the Si/Al molar ratio and increasing their relative crystallinity (Table 3) as expected. The lower total acid site concentration in the samples with a higher Al content (HBZ-3 and HBZ-4, Si/Al = 20 – 22) compared to HBZ-5 and HBZ-6 (Si/Al = 18 for both) can be explained by a higher fraction of the amorphous phase (ca. 10 – 15%, Table 1) in the first ones. Low acidity of amorphous aluminosilicate materials has been previously reported [46]. The low-crystalline samples HBZ-1 – HBZ-2 have predominantly strong Lewis acid sites (73 – 86% among total LAS, Table A.1), while the fractions of weak-to-medium (40 – 60% among total BAS) Brønsted acid sites are comparable to those in Al-rich HBZ-3-HBZ-6 series. The Brønsted-to--Lewis acid sites ratios BAS/LAS for low-crystalline Al-poor samples HBZ-1 and HBZ-2 are close to 1. Highly crystalline materials HBZ-3 – HBZ-6 possess a higher fraction of strong Brønsted acid sites (66 – 83%) compared to HBZ-1 and HBZ-2. For the sample with the highest relative crystallinity HBZ-5, the Brønsted acid site concentration is twofold higher than the Lewis acid site concentration.

3.2. Reactivity

Evaluation of the Weisz-Prater criterion for the most active catalyst exhibiting the highest value of TOF and thus the lowest final concentration for the substrate was done by assuming that the porosity to tortuosity ratio is ca. 0.1 for the catalyst particle radius of ca. 30 μm. The diffusion coefficient for the liquid was taken as 10^{-9} m^2/s. The value of the Weisz-Prater criterion of ca. $4{\cdot}10^{-3}$ clear indicates absence of the internal mass transfer limitations. Experiments performed at a higher stirring rate displayed the same conversion pointing out on the absence of external mass transfer limitations.

In the Prins cyclization between isoprenol and isovaleraldehyde over hierarchical beta zeolites, HBZ-3 and HBZ-2 catalysts displayed the highest conversion of isoprenol (ca. 80% after 3 h, Fig. 3).

Both HBZ-3 and HBZ-2 possess moderate acidity (Table 3), developed mesoporosity and the highest external surface area (Table 2). Consequently, HBZ-2 and HBZ-3 catalysts demonstrate the highest catalytic activity in terms of TOF values (Fig. 4a), reaction rates (Table 4) and CP3h (for HBZ-2) values (Fig. 4b).

The kinetic profiles of HBZ-4 and HBZ-6, which exhibited the lowest conversion values, clearly point out on catalyst deactivation as the activity rapidly declines after the first 30 min of the reaction.

The lowest initial activity of HBZ-1 (Fig. 3) might be related to the lowest concentration of acid sites in this catalyst.

While the selectivity towards pyranols maintained with increase in the conversion of isoprenol (Fig. 3b) up to ca. 30%, it elevated at higher

Table 3
Si/Al molar ratio in the samples and their acidity evaluated by pyridine adsorption with IR-spectral analysis.

Sample	Si/Al	C_B[a] (mmol/g)				C_L[b] (mmol/g)				C_Σ[c] (mmol/g)	*BAS/LAS*
		W[d]	M[e]	S[f]	Total	W	M	S	Total		
HBZ-1	46	0.03	0.01	0.06	0.10	0.03	0.00	0.08	0.11	0.21	0.9
HBZ-2	43	0.03	0.06	0.06	0.15	0.01	0.01	0.12	0.14	0.29	1.0
HBZ-3	20	0.00	0.06	0.22	0.28	0.04	0.01	0.16	0.21	0.49	1.3
HBZ-4	22	0.01	0.04	0.10	0.15	0.06	0.00	0.13	0.19	0.34	0.8
HBZ-5	18	0.07	0.01	0.39	0.47	0.04	0.00	0.18	0.22	0.69	2.1
HBZ-6	18	0.01	0.09	0.34	0.44	0.03	0.00	0.22	0.25	0.69	1.8

[a] Brønsted acid site concentration.
[b] Lewis acid site concentration.
[c] Total acid site concentration.
[d] Weak acid sites – pyridine is desorbed in the range of 150 – 250 °C.
[e] Medium acid sites – pyridine is desorbed in the range of 250 – 350 °C.
[f] Strong acid sites – pyridine remains adsorbed after desorption at 350 °C.

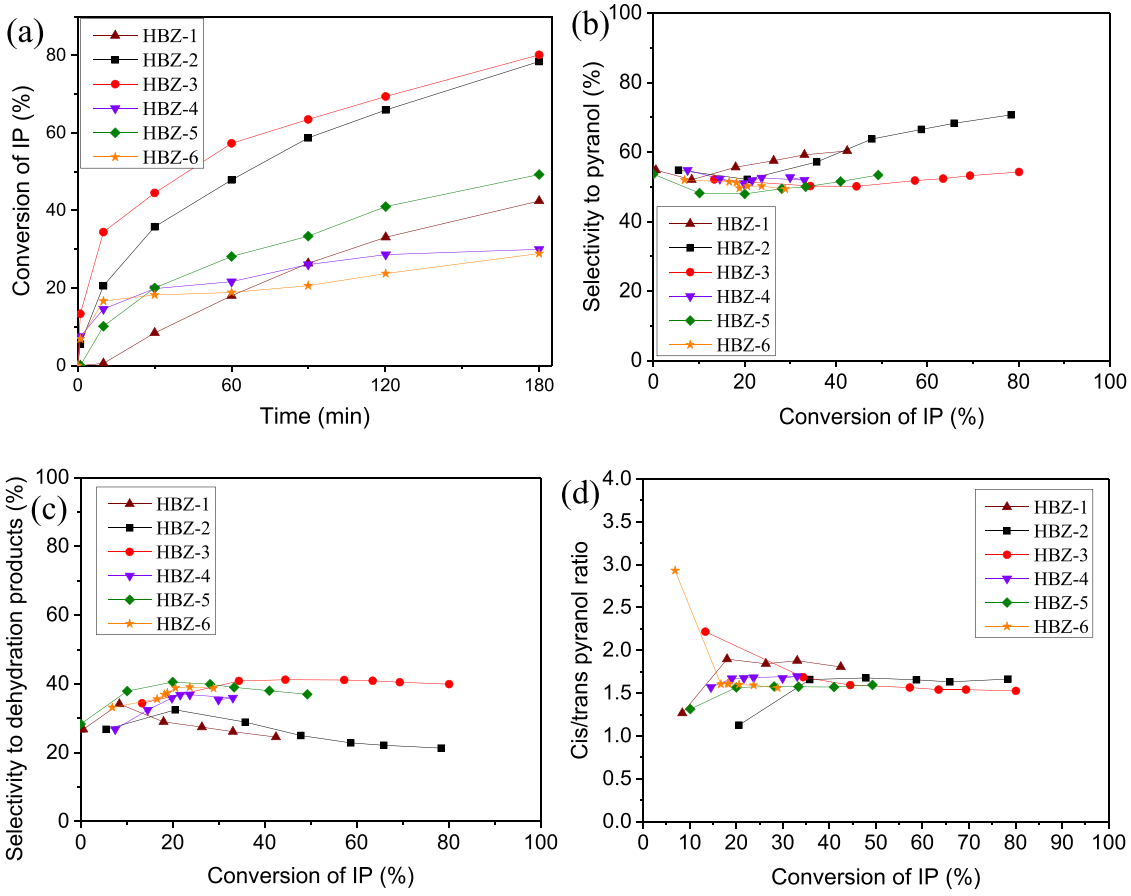

Fig. 3. Dependence of the conversion of isoprenol (IP) on the reaction time (a), selectivity to pyranol (b), *cis/trans* pyranol ratio (c) and selectivity to dehydration products (d) as a function of conversion over the prepared hierarchical beta zeolites.

conversions, especially for HBZ-2 and HBZ-3. Similar trends could be previously seen [31] for mesoporous USY materials, while for Beta-25 and Beta-38 selectivity to pyranol remained the same independent on conversion [31].

The highest selectivity (ca. 71%) was reached over HBZ-2 (Table 4), exceeding the values previously reported for Beta-25 and Beta-38 at complete conversion [31].

On the contrary, selectivity towards the dehydration products over hierarchical beta catalysts slightly decreases at higher conversion levels (Fig. 3c). This trend differs from the results reported earlier for microporous materials, where selectivity to dehydration products either maintained or just marginally increased with conversion. The reason of such trends in selectivity *vs* conversion values observed over hierarchical beta zeolites is provided *vide infra* when discussing the results of the kinetic analysis of the Prins reaction.

The *cis/trans* ratio of pyranol (Fig. 3d) is almost constant (ca. 1.6 – 1.7) at elevated conversion levels (>30%), being somewhat higher at lower conversions for two materials. Similarly, a decrease in the ratio of *cis/trans* pyranols from 2.25–3 to 1.8–2.5 was reported in [31] for microporous H-Beta zeolites with an increase in isoprenol conversion obviously due to more rapid transformations of the desired *cis* isomer over such materials compared to the *trans* one.

Analysis of the catalytic data as a function of acidity and structural properties of hierarchical beta zeolites is given in Fig. 5. Noticeably,

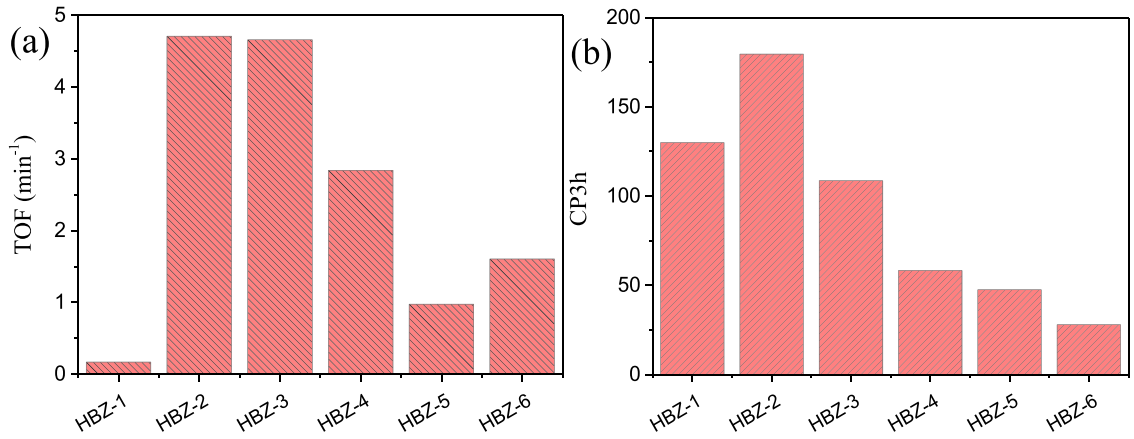

Fig. 4. TOF (a) and CP3h (b) obtained for the Prins cyclization between isoprenol and isovaleraldehyde over hierarchical beta zeolites.

Table 4
Catalytic performance of hierarchical beta zeolites in the Prins cyclization between isoprenol and isovaleraldehyde.

Catalyst	Initial reaction rate (mmol/min g_{cat})	Conversion of isoprenol after 3 h (%)	Selectivity to pyranol at 30% conversion (%)	Cis/trans pyranol ratio at 30% conversion (%)	Selectivity to dihydropyrans at 30% conversion (%)	Yield of pyranol after 3 h (%)
HBZ-1	0.01	42.4	58.4 (60.3)	1.9 (1.8)	26.6 (24.5)	25.6
HBZ-2	1.31	78.4	55.2 (70.7)	1.5 (1.7)	30.2 (21.3)	55.4
HBZ-3	2.28	80.1	50.4 (54.2)	1.8 (1.5)	39.3 (39.9)	43.4
HBZ-4	0.92	30.0	52.7 (52.7)	1.7 (1.7)	35.4 (35.4)	15.8
HBZ-5	0.64	49.3	49.5 (53.4)	1.6 (1.6)	39.3 (37.0)	26.3
HBZ-6	1.04	28.9	49.4[a] (49.4)	1.6[a] (1.6)	38.7[a] (38.7)	14.3

[a] at 28.9% conversion.
In parenthesis after 3 h.

selectivity towards the desired pyranol increases with the fraction of weak and medium Brønsted acid sites (Table A.1, Fig. 5a) and somewhat decreases for catalysts with a larger fraction of strong Brønsted acid sites (Fig. 5b). At the same time, selectivity towards dehydration products is increasing for materials with larger amounts of strong Brønsted acid sites (Table A.1, Fig. A.12a) pointing out that strong acid sites are more preferable for dehydration rather than formation of the desired pyranol.

An increase in the Brønsted-to-Lewis acid sites ratios (BAS/LAS) led to lower selectivity towards the desired pyranol (Fig. 5c) at the expense of the dehydration products (Fig. A.12b) indicating that the Brønsted acidity, especially the strong one, is unfavorable for formation of pyranols as indicated above. Such a trend could not be seen in the previous work covering H- and Fe-beta modified catalysts [31]. The revealed change of the pyranol selectivity with the BAS/LAS ratio (Fig. 5c) is obviously caused by the accompanying variations in the samples acidity, namely a considerable increase in the fraction of strong BAS for the catalysts with a higher BAS/LAS ratio (Table 3).

The *cis/trans* ratio of pyranols passed through a maximum as a function of strong Brønsted acid site fraction (Fig. 5d). Comparison of the obtained catalytic results with textural properties of the catalysts allowed to suggest a positive influence of the developed mesoporosity on the performance of hierarchical beta zeolites. In particular, for the series of Al-rich HBZ-3-HBZ-6 with similar Si/Al and BAS/LAS ratios and strength of acid sites, an increase of the fraction of mesopores in the total porosity is accompanied by a noticeable increase in the yield of pyranol (Fig. 5e). However, an increase of the mesopore size from ca. 10 to 30 nm is apparently not beneficial for the catalytic performance as visible in Fig. 5f. It should be mentioned that in this size range the cross-section of the reactants is obviously much less than the mesopore diameter allowing an easy access of the reactants to the active sites.

An apparent correlation between the external surface area and yield of the desired product (Fig. A.12c) testifies a favorable impact of the developed surface (other than microporous one) on the catalytic properties of the hierarchical zeolites. The DHP(A)/DHP(C) ratio demonstrates the trend of increasing with an increase of the fraction of micropores in the investigated zeolite samples (Fig. A.12d) being generally in accordance with the previous work where microporous catalysts were found to give higher DHP(A)/DHP(C) values than mesoporous samples [31]. Moreover, the values of the DHP(A)/DHP(C) ratio for the highest fraction of micropores was ca. 1.8 being somewhat lower than reported previously (2–2.5) for microporous beta zeolites.

To check reusability of the most active hierarchical beta catalyst, the spent HBZ-2 sample was tested in the second consecutive catalytic experiment after calcination at 400 °C. The obtained data (Fig. 6a) revealed that initial conversion of isoprenol over the spent sample is approximately the same within 30 min despite a lower (by 45%) catalyst loading in the reactor. Thereafter, in the second run the conversion level deteriorated and 60% conversion was reached at ca. 160 min, while 90 min were sufficient to get the same conversion level in the first run.

It should be noted, that the corresponding acetalization products (hemiacetal and acetal) were not formed over the studied zeolite catalysts, contrary to previously reported Fe-modified silica [27] and Beta zeolites [28], which can be related to lower acidity of the applied catalysts compared to the parent Beta zeolite.

3.3. Kinetic analysis

Based on the previous papers considering the mechanism of the Prins cyclization reaction [24,31] and the obtained dependencies of selectivity on isoprenol conversion over hierarchical beta zeolites, the reaction pathways presented in Scheme 2 can be suggested for the studied catalysts.

Isovaleraldehyde (IVA) is protonated over Brønsted acid sites with subsequent interactions of the generated protonated reagent **A** with an unsaturated alcohol isoprenol (IP) yielding the corresponding protonated hemiacetal **B**. This intermediate **B** through water elimination is transformed into an oxocarbenium ion **C,** which due to the presence of the double C–C bond and a positive charge on the O atom is capable of a

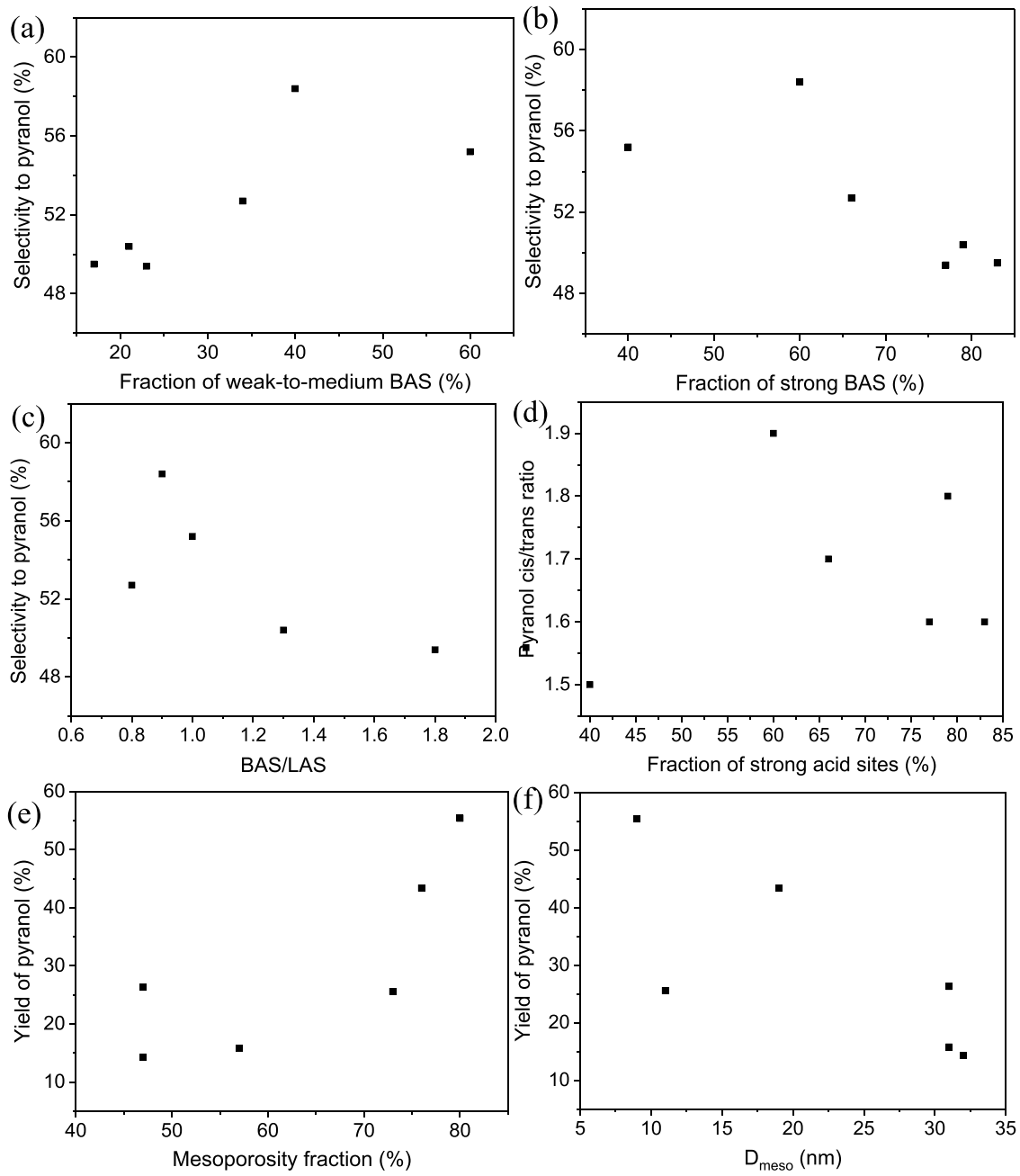

Fig. 5. Selectivity (at 30% conversion) of pyranol as a function of the fraction of weak and medium (a) and strong (b) Brønsted acid sites, the ratio of Brønsted and Lewis acid sites (c), *cis/trans* ratio of pyranols as a function of the fraction of strong Brønsted acid sites (d), yield of pyranol (after 3 h) as a function of the fraction of mesopores (e) and mesopore diameter (f) of the prepared zeolites.

further rapid cyclization generating a pyranol-type intermediate **D**. Interactions of the formed cation **D** with water result in the substituted tetrahydropyranol (THP). Considering the correlation of the selectivity to the desired pyranol with the fraction of weak and medium Brønsted acid sites (Fig. 5a) and an increase in the selectivity to THP with the conversion of IP (Fig. 3b), the route (a) is expected to proceed on these active sites. On the other hand, the carbocation **D** can be also subjected to proton elimination yielding three dihydropyrans (DHP). Dependence of the selectivity to the dehydration products on the fraction of strong Brønsted acid sites (Fig. 5b), as well as a decrease in selectivity towards the side products with conversion of IP (Fig. 3c) allow to suggest that the corresponding route (b) obviously requires strong acid sites which are gradually deactivating during the reaction. The obtained observations even being different from those reported for microporous zeolites are conceptually in line with the previous hypothesis [31] of the parallel rather than consecutive formation of the reaction products.

Kinetic analysis with numerical data fitting was performed to quantify the mechanistic considerations above and in particular to address the selectivity changes with conversion as a result of catalyst deactivation. The reaction network (Scheme 3) is a simplified version of a more mechanistically sound Scheme 2.

The network comprises parallel formation of THP and DHP with the reaction rates r_1 and r_2 as well as formation of trimers (r_3). For the kinetic modeling, the concentration IVA was assumed constant because of 5-fold excess of isovaleraldehyde with respect to isoprenol. Thus, the incorporation of IVA concentration to the lumped rate constant led to the following Eqs. (7)-(9)

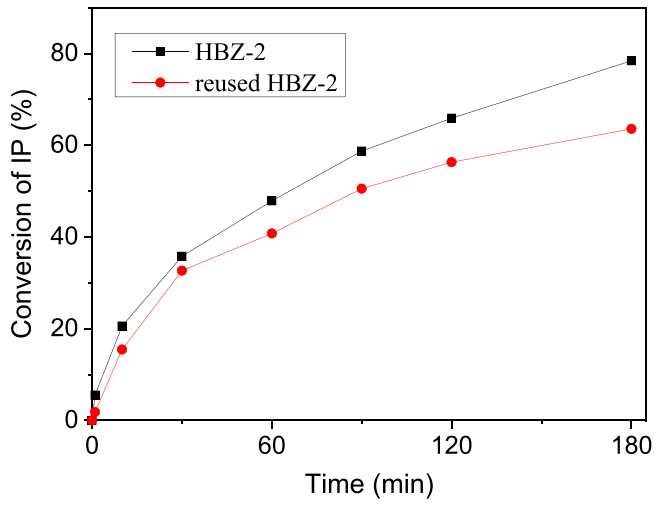

Fig. 6. Dependence of the conversion of isoprenol (IP) on the reaction time over fresh and spent catalyst HBZ-2.

$$r_1 = \frac{k_1 C_{IP}}{D} a_{weak/medium\_sites} \quad (7)$$

$$r_2 = \frac{k_2 C_{IP}}{D'} a_{strong\_sites} \quad (8)$$

$$r_3 = \frac{k_3 C_{DHP} C_{IP}}{D'} a_{strong\_sites} \quad (9)$$

where $k_1 - k_3$ are the rate constants for the corresponding reactions, D and D' are the denominators, reflecting presence of different adsorbed species on the sites of different strength. Preliminary calculations have demonstrated that the adsorption terms can be essentially neglected in line with close to almost first order kinetic curves giving $D = D' = 1$.

Deactivation was incorporated in the model by time dependent activity of acid sites of different nature, i.e.

$$a_{weak/medium\_sites,t} = e^{-k_{d,weak/medium} t} \quad (10)$$

$$a_{strong\_sites,t} = e^{-k_{d,strong} t} \quad (11)$$

where $k_{d,weak/medium}$ and $k_{d,strong}$ are the deactivation constants on weak/medium and strong sites respectively, t is time.

The differential equations addressing the mass balances for different compounds

$$\frac{dC_{IP}}{dt} = -r_1 - r_2 \quad (12)$$

$$\frac{dC_{THP}}{dt} = r_1 \quad (13)$$

$$\frac{dC_{DHP}}{dt} = r_2 - r_3 \quad (14)$$

$$\frac{dC_{TRI}}{dt} = r_3 \quad (15)$$

were solved using the backward difference method. The simplex and Levenberg–Marquardt methods were used for the parameter estimation performed using the optimization and simulation software ModEst [47]. The estimated rate constants and calculated concentrations are shown in Fig. 7 and in Table 5 for Al-rich catalytic materials. The value of the coefficient of determination R^2, defined as the variance of all experimental points from the mean value, was exceeding 97–99%, thus confirming an adequate description of experimental data.

Large differences in the values of deactivation constants on weak/medium and strong sites reflect changes of selectivity with conversion as strong acid sites deactivate in a more profound way during the reaction.

3.4. Role of water

As has been demonstrated [48], the addition of water (in a moderate

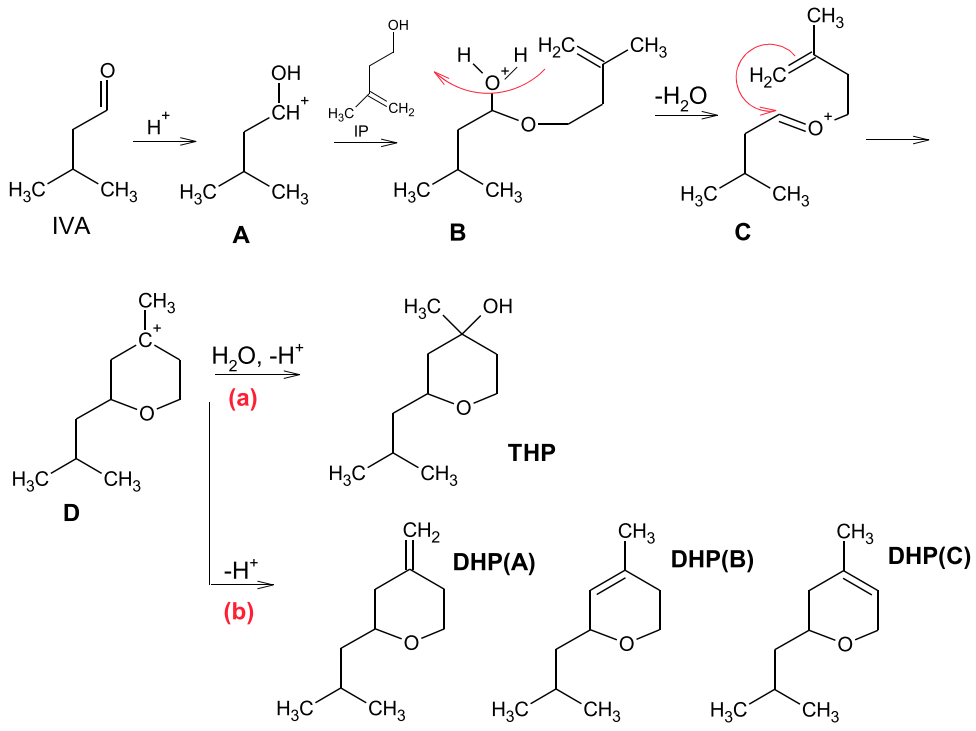

Scheme 2. A plausible mechanism of Florol formation from isovaleraldehyde and isoprenol over beta zeolites. Route (a) proceeds mostly over weak-to-medium Brønsted acid sites, while route (b) requires strong Brønsted acid sites.

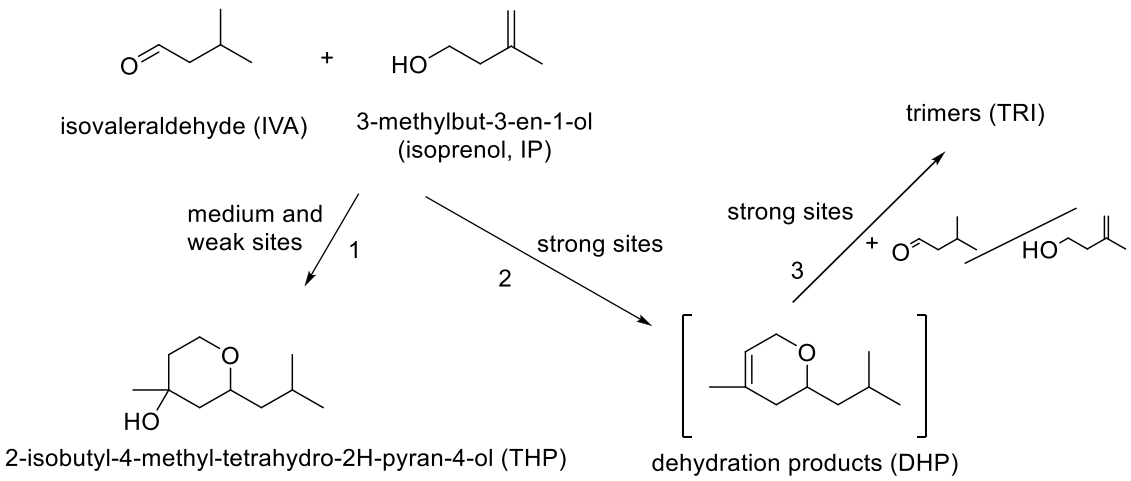

Scheme 3. Reaction network of Florol formation from isovaleraldehyde and isoprenol over beta zeolites.

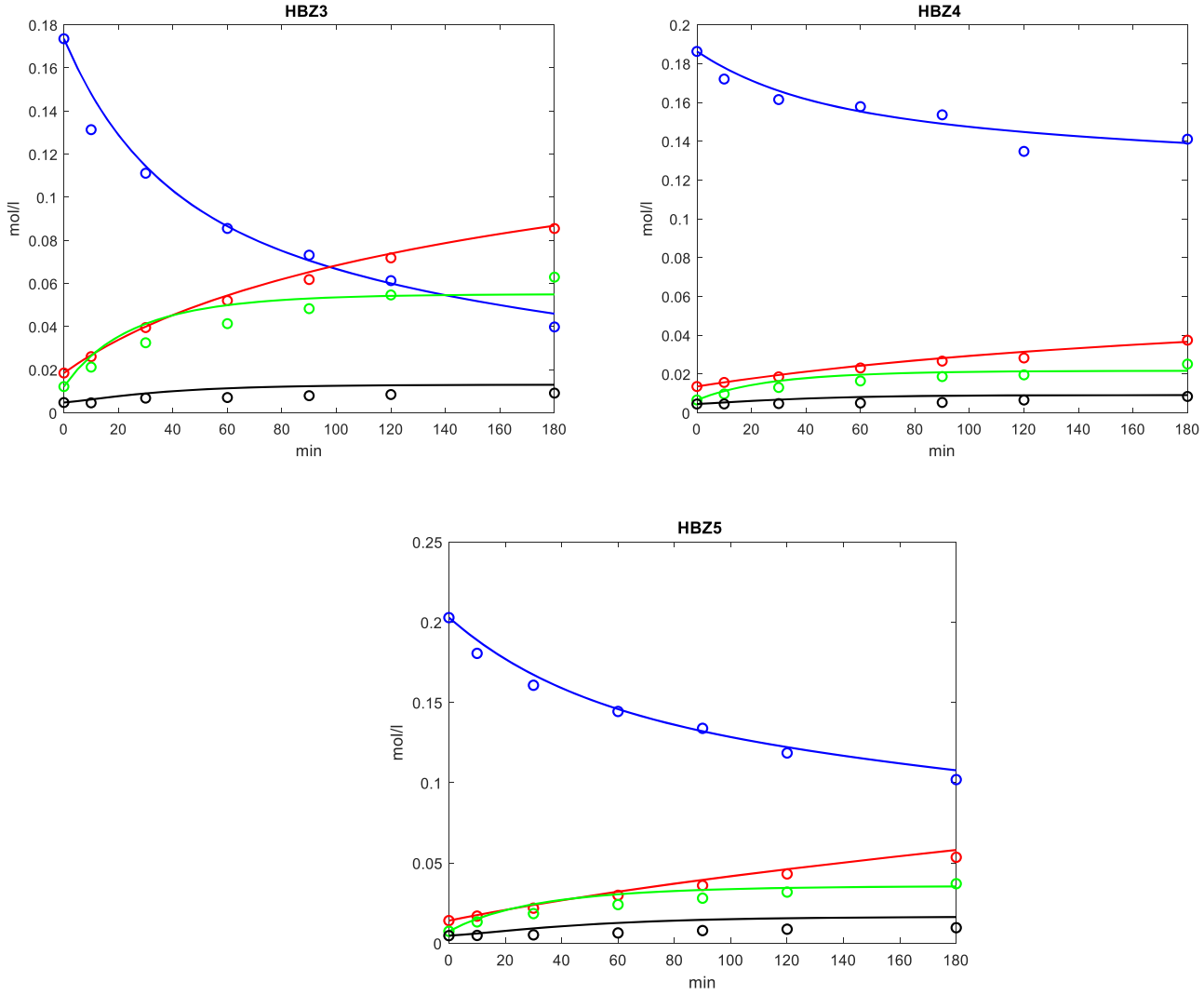

Fig. 7. Comparison between experimental (symbols) and calculated (lines) concentrations of reactants and products in Florol synthesis. Notation: (blue) IP, (red) THP, (green) DHP, (black) TRI.

amount) to the reaction mixture consisting of isoprenol, isovaleraldehyde and a catalyst with sulfuric or sulfonic groups (sulfuric acid, Amberlyst 15, *p*-toluenesulfonic and *p*-dodecylbenzenesulfonic acids) leads to a significant increase in the catalytic performance, namely the reaction rate and selectivity towards substituted tetrahydropyranol. Such effect of water was associated with the suppression of a

Table 5
The estimated rate constants for Florol synthesis according to Scheme 3.

Parameter	HBZ3 Estimate	(R^2=97.4%) St. error (%)	HBZ4 Estimate	(R^2=99.7%) St. error (%)	HBZ5 Estimate	(R^2=99.3%) St. error (%)
k_1, (min^{-1})	5.25×10^{-3}	105	1.22×10^{-3}	28	1.78×10^{-3}	22
k_2, (min^{-1})	0.011	104	3.42×10^{-3}	30	5.17×10^{-3}	20
k_3 (L $mol^{-1}min^{-1}$)	0.051	10	0.055	44	0.067	28
$k_{d,weak/medium}$ (min^{-1})	1.66×10^{-3}	>100	4.68×10^{-3}	99	1.16×10^{-4}	>100
$k_{d,strong}$ (min^{-1})	0.025	68	0.029	40	0.021	30

side dehydration reaction. The role of water was also found to be essential for halloysite nanotubes as a stereoselective catalyst for synthesis octahydro-2*H*-chromen-4-ol [49]. In particular, removal of water by drying the catalyst at elevated temperature was detrimental for selectivity to the desired chromenols. The previous research on Beta and USY zeolites as catalysts for this reaction [31] demonstrated promising catalytic performance of dried (overnight at 100 °C), i.e. still water-containing samples, instead of activated ones as applied typically in catalysis with zeolite.

In contrast to previously reported results, in particular using conventional zeolites, the presence of pre-adsorbed and/or structural water was not favorable in the current study using hierarchical zeolites. As can be seen from the comparative results with water-containing and water-free catalysts the latter displayed higher (sample HBZ-1) or similar (samples HBZ-2 and HBZ-6) catalytic activity compared to water-containing samples (Fig. 8). Therefore, upon using zeolites, in contrast to other studied catalysts, even a low water amount precludes the desired cyclization, most likely due to significant blocking of the acid sites with water. Much lower initial catalytic activity of wet vs water-free HBZ-1 contrasted to similar reactivity of wet and water-free HBZ-2 and HBZ-6 samples. Stronger deactivation of HBZ-1 with water can be attributed to a higher microporosity fraction of HBZ-1 compared to HBZ-2 resulting therefore in stronger adsorption of water on active sites located in the micropores possessing high adsorption potential. Additionally, absence of the water effect for HBZ-6 can be connected with its mesopores, which are 3-fold larger compared to HBZ-1 (ca. 32 nm vs. 11 nm, Table 2). This allows easier water desorption and accessibility of the acid sites located on the mesopore surface mitigating their blocking with water. In general, it seems to be challenging enough to predict the influence of water on catalytic activity of hierarchical zeolites clearly considering variations of their textural and acidic parameters in a broad range.

As far as the Prins cyclization is concerned, generation of mesoporosity in zeolites was found to be crucial for small-pore materials such as, for instance, ZSM-5, which was not active in the Prins reaction of (-)-isopulegol with benzaldehyde, while micro-mesoporous catalysts based on this zeolite demonstrated high catalytic performance [50]. In the case of comparatively large-pore beta zeolites additional mesoporosity turned out to be not such a crucial factor as acidic characteristics. In particular, commercial beta zeolites were found to be active and selective (up to 72%) towards pyranol formation at almost complete (up to 99%) conversion of isoprenol obviously due to the developed porous structure [31]. The experimental procedure reported herein for the synthesis of hierarchical beta zeolites allows fine-tuning not only textural but also acidic characteristics, i.e. strength and concentration of the acid sites, which are responsible for catalytic performance of such materials.

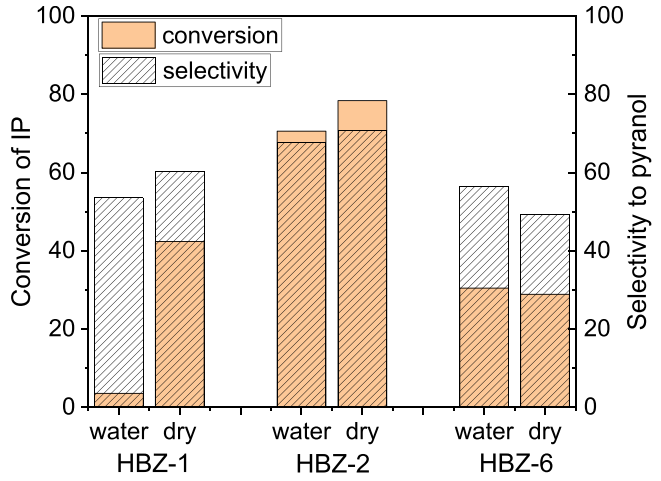

Fig. 8. Catalytic behavior of selected wet and dried catalysts in the Prins cyclization of isoprenol and isovaleraldehyde.

4. Conclusions

Several hierarchical beta zeolites synthesized *via* a simple and a straightforward method in alkali metal-free protic acid-containing mixtures were studied in Prins cyclization of isovaleraldehyde and isoprenol under mild reaction conditions (40 °C) using a sustainable green solvent (dimethylcarbonate). The highest yield of the desired tetrahydropyranol (a commercial perfume ingredient Florol) was obtained using hierarchical beta zeolite consisting of relatively small nanoparticles (ca. 20 nm) agglomerated in larger ones. This material possesses developed mesoporosity (V_{meso} 0.60 cm^3/g, S_{ext} 290 m^2/g) at the expense of a decreased micropore volume (V_{micro} 0.15 cm^3/g) enhancing accessibility of the active sites. Application of zeolites with moderate acidity and a low Brønsted-to-Lewis acid sites ratio (up to 1) allows obtaining higher selectivity towards the desired substituted tetrahydropyranol. Based on the generated experimental results and available literature data, a preferable formation of substituted tetrahydropyranol over weak and medium Brønsted acid sites, on the one hand, and generation of dehydration products mainly over strong Brønsted acid sites, on the other hand, proceeding in parallel routes were suggested. The mechanistic scheme was supported by kinetic modeling, which incorporated deactivation of acid sites to a different extent depending on their strength.

CRediT authorship contribution statement

Nataliya Shcherban: Investigation, Supervision, Writing – original draft, Writing – review & editing. **Roman Barakov:** Investigation, Writing – review & editing. **Basile Lasne:** Investigation. **Päivi Mäki-Arvela:** Conceptualization, Supervision, Writing – review & editing. **Mariya Shamzhy:** Investigation, Writing – review & editing. **Igor Bezverkhyy:** Investigation. **Johan Wärnå:** Investigation. **Dmitry Yu. Murzin:** Supervision, Writing – review & editing.

Declaration of Competing Interest

The authors declare that they have no known competing financial interests or personal relationships that could have appeared to influence the work reported in this paper.

Data availability

Data will be made available on request.

Acknowledgment

The authors are grateful to Prof. Jiří Čejka and CSc. Maksym Opanasenko (Charles University, Prague) for discussing the results. N.S. and R.B. acknowledge the support of the National Research Foundation of Ukraine to the project "New effective zeolite catalysts for environmentally friendly processes of the conversion of renewable raw materials into valuable organic compounds" (project number 2020.02/0335). M. S. acknowledges the Czech Science Foundation for supporting this work through project 20-12099S. The authors express their gratitude to Prof. Roman Bulánek (University of Pardubice) for collecting ICP-OES analysis data and Ph.D. Martin Kubů (Charles University, Prague) for nitrogen adsorption measurements.

Supplementary materials

Supplementary material associated with this article can be found, in the online version, at doi:10.1016/j.mcat.2022.112683.

References

[1] W. Schwieger, A.G. Machoke, T. Weissenberger, A. Inayat, T. Selvam, M. Klumpp, A. Inayat, Hierarchy concepts: classification and preparation strategies for zeolite containing materials with hierarchical porosity, Chem. Soc. Rev. 45 (2016) 3353–3376, https://doi.org/10.1039/C5CS00599J.
[2] J. Prech, P. Pizarro, D.P. Serrano, J. Cejka, From 3D to 2D zeolite catalytic materials, Chem. Soc. Rev. 47 (2018) 8263–8306, https://doi.org/10.1039/C8CS00370J.
[3] J. Čejka, R. Millini, M. Opanasenko, D.P. Serrano, W.J. Roth, Advances and challenges in zeolite synthesis and catalysis, Catal. Today 345 (2020) 2–13, https://doi.org/10.1016/j.cattod.2019.10.021.
[4] M. Hartmann, M. Thommes, W. Schwieger, Hierarchically-ordered zeolites: a critical assessment, Adv. Mater. Interfaces 8 (2021), 2001841, https://doi.org/10.1002/admi.202001841.
[5] D.H. Park, S.S. Kim, H. Wang, T.J. Pinnavaia, M.C. Papapetrou, A.A. Lappas, K. S. Triantafyllidis, Selective petroleum refining over a zeolite catalyst with small intracrystal mesopores, Angew. Chem. Int. Ed. Engl. 48 (2009) 7645–7648, https://doi.org/10.1002/ange.200901551.
[6] S. Soltanali, J.T. Darian, Synthesis of mesoporous beta catalysts in the presence of carbon nanostructures as hard templates in MTO process, Microporous Mesoporous Mater. 286 (2019) 169–175, https://doi.org/10.1016/j.micromeso.2019.05.013.
[7] X. Li, Y. Shi, Z. Wang, Y. Zhang, Y. Tang, Catalytic performance of H-β nanozeolite microspheres in one-pot dynamic kinetic resolution of aromatic sec-alcohols, J. Catal. 288 (2012) 24–32, https://doi.org/10.1016/j.jcat.2011.12.021.
[8] J. Zhu, Y. Zhu, L. Zhu, M. Rigutto, A. van der Made, C. Yang, S. Pan, L. Wang, L. Zhu, Y. Jin, Q. Sun, Q. Wu, X. Meng, D. Zhang, Y. Han, J. Li, Y. Chu, A. Zheng, S. Qiu, X. Zheng, F.S. Xiao, Highly mesoporous single-crystalline zeolite beta synthesized using a nonsurfactant cationic polymer as a dual-function template, J. Am. Chem. Soc. 136 (2014) 2503–2510, https://doi.org/10.1021/ja411117y.
[9] M. Choi, H.S. Cho, R. Srivastava, C. Venkatesan, D.H. Choi, R. Ryoo, Amphiphilic organosilane-directed synthesis of crystalline zeolite with tunable mesoporosity, Nat. Mater. 5 (2006) 718–723, https://doi.org/10.1038/nmat1705.
[10] J.M. Escola, D.P. Serrano, R. Sanz, R.A. Garcia, A. Peral, I. Moreno, M. Linares, Synthesis of hierarchical Beta zeolite with uniform mesopores: effect on its catalytic activity for veratrole acylation, Catal. Today 304 (2018) 89–96, https://doi.org/10.1016/j.cattod.2017.08.005.
[11] K. Na, C. Jo, J. Kim, K. Cho, J. Jung, Y. Seo, R.J. Messinger, B.F. Chmelka, R. Ryoo, Directing zeolite structures into hierarchically nanoporous architectures, Science 333 (2011) 328–332, https://doi.org/10.1126/science.1204452.
[12] R. Barakov, N. Shcherban, P. Yaremov, I. Bezverkhyy, J. Čejka, M. Opanasenko, Hierarchical beta zeolites as catalysts in a one-pot three-component cascade Prins–Friedel–Crafts reaction, Green Chem. 22 (2020) 6992–7002, https://doi.org/10.1039/D0GC01787F.
[13] X. Wang, Y.X. Li, C. Luo, J. Liu, B.H. Chen, Direct synthesis of hierarchical zeolites with oriented nanocrystals without adding extra templates, RSC Adv. 3 (2013) 6295–6298, https://doi.org/10.1039/C3RA21913E.
[14] K. Möller, B. Yilmaz, U. Müller, T. Bein, Nanofusion: mesoporous zeolites made easy, Chem. Eur. J. 18 (2012) 7671–7674, https://doi.org/10.1002/chem.201200544.
[15] R. Barakov, N. Shcherban, P. Yaremov, I. Bezverkhyy, V. Tsyrina, M. Opanasenko, Hierarchical Beta zeolites obtained in concentrated reaction mixtures as catalysts in tetrahydropyranylation of alcohols, Appl. Catal. A Gen. 594 (2020), 117380, https://doi.org/10.1016/j.apcata.2019.117380.
[16] W. Zhang, W. Ming, S. Hu, B. Qin, J. Ma, R. Li, A feasible one-step synthesis of hierarchical zeolite Beta with uniform nanocrystals via CTAB, Mater. (Basel) 651 (11) (2018), https://doi.org/10.3390/ma11050651.
[17] M. Laluc, R. Barakov, P. Mäki-Arvela, N. Shcherban, D.Y. Murzin, Catalytic activity of hierarchical beta zeolites in the Prins cyclization of (-)-isopulegol with acetone, Appl. Catal. A Gen. 618 (2021), 118131, https://doi.org/10.1016/j.apcata.2021.118131.
[18] R. Barakov, N. Shcherban, P. Mäki-Arvela, P. Yaremov, I. Bezverkhyy, J. Wärnå, D. Y. Murzin, Hierarchical Beta zeolites as catalysts in α-pinene oxide isomerization, ACS Sustain. Chem. Eng. 10 (2022) 6642–6656, https://doi.org/10.1021/acssuschemeng.2c00441.
[19] F. Doro, N. Akeroyd, F. Schiet, A. Narula, The Prins reaction in the fragrance industry: 100th anniversary (1919–2019), Angew. Chem. 131 (2019) 7248–7253, https://doi.org/10.1002/ange.201814470.
[20] C. Sell, Ingredients for the modern perfumery industry, in: C. Sell (Ed.), The Chemistry of Fragrances. From Perfumer to Consumer, RSC Publishing, Cambridge, 2006, pp. 52–131.
[21] G.P. More, M. Rane, S.V. Bhat, Efficient Prins cyclization in environmentally benign method using ion exchange resin catalyst, Green Chem. Lett. Rev. 5 (2012) 13–17, https://doi.org/10.1080/17518253.2011.572929.
[22] L. Sekerová, P. Březinová, T.T. Do, E. Vyskočilová, J. Krupka, L. Červený, L. Havelková, B. Bashta, J. Sedláček, Sulfonated hyper-cross-linked porous polyacetylene networks as versatile heterogeneous acid catalysts, ChemCatChem 12 (2020) 1075–1084, https://doi.org/10.1002/cctc.201901815.
[23] E. Vyskočilová, M. Krátká, M. Veselý, E. Vrbková, L. Červený, Prins cyclization for the preparation of 2-isobutyl-4-methyl-tetrahydro-2H-pyran-4-ol using supported heteropoly acids, Res. Chem. Intermed. 42 (2016) 6991–7003, https://doi.org/10.1007/s11164-016-2511-1.
[24] A.L. de Meireles, K.A. da Silva Rocha, E.F. Kozhevnikova, I.V. Kozhevnikov, E. V. Gusevskaya, Heteropoly acid catalysts in Prins cyclization for the synthesis of Florol®, Mol. Catal. 502 (2021), 111382 https://doi.org/10.1016/j.mcat.2020.111382.
[25] L. Sekerová, E. Vyskočilová, L. Červený, Prins cyclization of isoprenol with various aldehydes using MoO_3/SiO_2 as a catalyst, React. Kinet. Mech. Catal. 121 (2017) 83–95, https://doi.org/10.1007/s11144-016-1131-5.
[26] E. Vyskočilová, L. Sekerová, I. Paterová, J. Krupka, M. Veselý, L. Červený, Characterization and use of MoO_3 modified alumosilicates in Prins cyclization of isoprenol and isovaleraldehyde, J. Porous Mater. 25 (2018) 273–281, https://doi.org/10.1007/s10934-017-0440-z.
[27] L. Sekerová, E. Vyskočilová, J.S. Fantova, I. Paterová, J. Krupka, L. Červený, Preparation of 2-isobutyl-4-methyltetrahydro-2H-pyran-4-ol via Prins cyclization using Fe-modified silica, Res. Chem. Intermed. 43 (2017) 4943–4958, https://doi.org/10.1007/s11164-017-2922-7.
[28] E. Vrbková, L. Sekerová, E. Vyskočilová, M. Zapletal, L. Červený, Iron-modified zeolite BETA: efficient catalyst in methyllaurate, 2-hexyl-1, 3-dioxolane, 4-methyl-2-propyltetrahydro-2H-pyran-4-ol and 4-methyl-2-phenyl-tetrahydro-2H-pyran-4-ol synthesis, Res. Chem. Intermed. 48 (2022) 1403–1421, https://doi.org/10.1007/s11164-022-04671-3.
[29] E. Vyskočilová, A. Gruberová, M. Shamzhy, E. Vrbková, J. Krupka, L. Červený, Prins cyclization in 4-methyl-2-phenyl-tetrahydro-2H-pyran-4-ol preparation using smectite clay as catalyst, React. Kinet. Mech. Catal. 124 (2018) 711–725, https://doi.org/10.1007/s11144-018-1371-7.
[30] A.Y. Sidorenko, Y.M. Kurban, A. Aho, Z.V. Ihnatovich, T.F. Kuznetsova, I. Heinmaa, D.Yu. Murzin, V.E. Agabekov, Solvent-free synthesis of tetrahydropyran alcohols over acid-modified clays, Mol. Catal. 499 (2021), 111306, https://doi.org/10.1016/j.mcat.2020.111306.
[31] B. Lasne, P. Mäki-Arvela, A. Aho, Z. Vajglova, K. Eränen, N. Kumar, J.E. Sánchez-Velandia, M. Peurla, C. Mondelli, J. Pérez-Ramírez, D.Yu. Murzin, Synthesis of Florol via Prins cyclization over heterogeneous catalysts, J. Catal. 405 (2022) 288–302, https://doi.org/10.1016/j.jcat.2021.12.008.
[32] M.A. Camblor, A. Corma, S. Valencia, Characterization of nanocrystalline zeolite Beta, Microporous Mesoporous Mater. 25 (1998) 59–74, https://doi.org/10.1016/S1387-1811(98)00172-3.
[33] J.W.M. Osterrieth, J. Rampersad, D. Madden, et al., How reproducible are surface areas calculated from the BET equation? Adv. Mater. 34 (2022), 2201502 https://doi.org/10.1002/adma.202201502.
[34] E.P. Barrett, L.G. Joyner, P.P. Halenda, The determination of pore volume and area distributions in porous substances. I. Computations from nitrogen isotherms, J. Am. Chem. Soc. 73 (1951) 373–380, https://doi.org/10.1021/ja01145a126.
[35] A. Galarneau, F. Villemot, J. Rodriguez, F. Fajula, B. Coasne, Validity of the t-plot method to assess microporosity in hierarchical micro/mesoporous materials, Langmuir 30 (2014) 13266–13274, https://doi.org/10.1021/la5026679.
[36] A. Galarneau, D. Mehlhorn, F. Guenneau, B. Coasne, F. Villemot, D. Minoux, C. Aquino, J.P. Dath, Specific surface area determination for microporous/mesoporous materials: the case of mesoporous FAU-Y zeolites, Langmuir 34 (2018) 14134–14142, https://doi.org/10.1021/acs.langmuir.8b02144.
[37] L. Desmurs, A. Galarneau, C. Cammarano, V. Hulea, C. Vaulot, H. Nouali, B. Lebeau, T.J. Daou, C.V. Soares, G. Maurin, M. Hananczyk, I. Batonneau, A. Sachse, ChemNanoMat 8 (2022), e202200051, https://doi.org/10.1002/cnma.202200051.
[38] M. Jaroniec, M. Kruk, J.P. Olivier, Standard nitrogen adsorption data for characterization of nanoporous silicas, Langmuir 15 (1999) 5410–5413, https://doi.org/10.1021/la990136e.
[39] C. Yang, Z. Dong, W. Chu, Y. Wang, D. Zhao, F. Chen, W. Xin, X. Zhu, S. Liu, L. Xu, Understanding the roles of different acid sites in beta zeolites with different particle sizes catalyzed liquid-phase transalkylation of diethylbenzene with

benzene, Catal. Sci. Technol. 12 (2022) 652–663, https://doi.org/10.1039/D1CY01849C.
[40] V. Zholobenko, C. Freitas, M. Jendrlin, P. Bazin, A. Travert, F. Thibault-Starzyk, Probing the acid sites of zeolites with pyridine: quantitative AGIR measurements of the molar absorption coefficients, J. Catal. 385 (2020) 52–60, https://doi.org/10.1016/j.jcat.2020.03.003.
[41] S. Mintova, N. Barrier, Verified Synthesis of Zeolitic Materials, 3rd ed., Elsevier, Amsterdam, 2016.
[42] A. Petushkov, G. Merilis, S.C. Larsen, From nanoparticles to hierarchical structures: controlling the morphology of zeolite beta, Microporous Mesoporous Mater. 143 (2011) 97–103, https://doi.org/10.1016/j.micromeso.2011.02.012.
[43] M. Thommes, K. Kaneko, A.V. Neimark, J.P. Olivier, F. Rodriguez-Reinoso, J. Rouquerol, K.S.W. Sing, Physisorption of gases, with special reference to the evaluation of surface area and pore size distribution (IUPAC Technical Report), Pure Appl. Chem. 87 (2015) 1051–1069, https://doi.org/10.1515/pac-2014-1117.
[44] J.C. Groen, L.A.A. Peffer, J. Pérez-Ramírez, Pore size determination in modified micro- and mesoporous materials. Pitfalls and limitations in gas adsorption data analysis, Microporous Mesoporous Mater. 60 (2003) 1–17, https://doi.org/10.1016/S1387-1811(03)00339-1.
[45] Y. Liu, T.J. Pinnavaia, Aluminosilicate mesostructures with improved acidity and hydrothermal stability, J. Mater. Chem. 12 (2002) 3179–3190, https://doi.org/10.1039/B204094H.
[46] E.G. Vaschetto, G.A. Monti, E.R. Herrero, S.G. Casuscelli, G.A. Eimer, Influence of the synthesis conditions on the physicochemical properties and acidity of Al-MCM-41 as catalysts for the cyclohexanone oxime rearrangement, Appl. Catal. A Gen. 453 (2013) 391–402, https://doi.org/10.1016/j.apcata.2012.12.016.
[47] H. Haario, ModEst, Software for Parameter Estimation, Helsinki, 2001.
[48] E. Vyskočilová, L. Rezková, E. Vrbková, I. Paterová, L. Červený, Contribution to elucidation of the mechanism of preparation of 2-isobutyl-4-methyltetrahydro-2H-pyran-4-ol, Res. Chem. Intermed. 42 (2016) 725–733, https://doi.org/10.1007/s11164-015-2052-z.
[49] E. Kholkina, P. Mäki-Arvela, C. Lozachmeuer, R. Barakov, N. Shcherban, D. Y. Murzin, Prins cyclisation of (–)-isopulegol with benzaldehyde over ZSM-5 based micro-mesoporous catalysts for production of pharmaceuticals, Chin. J. Catal. 40 (2019) 1713–1720, https://doi.org/10.1016/S1872-2067(19)63305-X.
[50] A.Yu. Sidorenko, A.V. Kravtsova, A. Aho, I. Heinmaa, J. Wärnå, H. Pazniak, K. P. Volcho, N.F. Salakhutdinov, D.Yu. Murzin, V.E. Agabekov, Highly selective Prins reaction over acid-modified halloysite nanotubes for synthesis of isopulegol-derived 2H-chromene compounds, J. Catal. 374 (2019) 360–377, https://doi.org/10.1016/j.jcat.2019.05.009.